Effect of supercritical carbonation on porous structure and mechanical strength of cementitious materials modified with bacterial nanocellulose

Juan Cruz Barría, Diego Manzanal, Siavash Ghabezloo, Jean-Michel Pereira

Effect of supercritical carbonation on porous structure and mechanical strength of cementitious materials modified with bacterial nanocellulose.

Juan Cruz Barría[1,3], Diego Manzanal[1,2,*], Siavash Ghabezloo[3], Jean-Michel Pereira[3]

[1] Facultad de Ingeniería, Universidad Nacional de la Patagonia San Juan Bosco, 9004 Comodoro Rivadavia, Chubut, Argentina.

[2] E.T.S.I. Caminos, Universidad Politécnica de Madrid, Prof. Aranguren 3, 28040 Madrid, Spain.

[3] Navier, Ecole des Ponts, Univ Gustave Eiffel, CNRS, Marne-la-Vallée, France.

*Correspondence to d.manzanal@upm.es

Abstract

The effect of wet supercritical CO_2 (90 °C and 20 MPa) on the performance of cement paste (PC) modified with bacterial nanocellulose (BNC) was investigated. The pore structure of carbonated cement shows a clogging over the outer rim of the samples. In contrast, near the sample core, the characteristic peak of pore size distribution shifted towards smaller pores analyzed by mercury intrusion porosimetry. The effect of the carbonation overtime on mechanical properties shows increasing alteration. XRD results show more crystalline phases of hydrated cement in the BNC samples before carbonation. Cement reinforced with BNC shows lower density, a reduction in its porosity, and experiences fewer porosity changes at the cement core. Furthermore, its mechanical performance was less affected by the carbonation process.

Keywords

Cement paste – Bacterial nanocellulose – Cement carbonation – Porosity – Mechanical Strength

1. Introduction

Global carbon dioxide (CO_2) emissions to the atmosphere are growing year after year [1]. Although new technologies are being developed to replace fossil fuels, humankind is still dependent on them. During this transition, reducing greenhouse gas emissions will be

crucial. Nowadays, there are several ways to increase the amount of carbon sinks in the world [2,3]. One of these methods relies on CO_2 geological storage [4], by which significant amounts of CO_2 can be stored in geological reservoirs [5,6].

Inside injection well, a cement sheath is placed between the casing and the formation rocks during the well completion to ensure stability, protect the casing against corrosion, and, most importantly, ensure wellbore sealing and zonal isolation. Along with the caprock, the cement sheath constitutes the hydraulic barrier against CO_2 leakage when injection is finished [7]. However, in presence of CO_2, carbonation of the cementitious materials is enhanced by the high pressure and high temperature conditions. The carbonation process affects the mechanical properties and permeability of the cement paste and may alter its role in ensuring the sealing and zonal isolation [8].

When injected in a geological reservoir, CO_2 first dissolves in the aqueous phase, generating carbonic acid (H_2CO_3). It then dissociates into bicarbonate (HCO_3^-) and carbonate ions (CO_3^{2-}), which in turn react with the hydrated cement compounds:

$$CO_2 + H_2O \leftrightarrow H_2CO_3 \leftrightarrow H^+ + HCO_3^- \quad (1)$$

$$HCO_3^- \leftrightarrow H^+ + CO_3^{2-} \quad (2)$$

The two main cement components react chemically with CO_2. The carbonation of saturated cement samples is considered to be diffusion-dominated processes [9]. Both reactions lead to the precipitation of calcium carbonate ($CaCO_3$) in its various forms (calcite, aragonite, or vaterite). The first cement component to react is calcium hydroxide (Portlandite):

$$Ca(OH)_2 + CO_2 \rightarrow CaCO_3 + H_2O \quad (3)$$

The drop in pH then allows the hydrated calcium silicate (C-S-H) to be decalcified in contact with CO_2. New studies have demonstrated that C-S-H carbonation does not release water, and the only effect is C-S-H decalcification and amorphous silica ($SiO_2 \cdot zH_2O(am)$) formation [10]:

$$C_{1.7} - S - H_z + 1.7\ CO_2 \rightarrow 1.7\ CaCO_3 + SiO_2 \cdot zH_2O(am) \quad (4)$$

57 Nevertheless, it has been found that dissolution of portlandite (CH) and C-S-H occurs
58 simultaneously [10,11].
59 Since C-S-H is the compound with most important influence on the cement mechanical
60 characteristics, its loss will reduce cement mechanical strength and could compromise the
61 wellbore integrity, while the reduction of pH may induce corrosion of the steel casing.
62 Cement carbonation produces a leaching front, which is characterized by an increase in
63 porosity, followed by a $CaCO_3$ precipitation zone of low porosity [12], and finally, near the
64 exposed front, a degraded zone of low pH, high porosity, and low strength is generated
65 (brown color zone) [13]. These fronts are of variable penetration and thickness, depending
66 on the cement curing conditions [14] and density [15].
67 The pressure and temperature in the geological reservoirs considered for CO_2 storage are
68 above the critical point for CO_2 (31.6 °C and 7.3 MPa). These conditions result in a high
69 CO_2 content per unit volume and a gas-like viscosity, which accelerate the carbonation
70 process of the cement. This barrier constituted by calcium carbonates can also be
71 dissolved by the CO_2–rich environment surrounding the cement sheath, which would
72 increase its porosity again [13,16–18].
73 The porosity development of cement during hydration depends mainly on the water to
74 cement ratio and the curing conditions. Cement with a higher hydration degree has lower
75 porosity for a given curing temperature, and therefore lower advection and diffusion
76 parameters [19,20].
77 Previous studies have shown that the incorporation of nanocellulose modifies the
78 mechanical properties, thermal stability, viscosity, and hydration degree of cement [21–25].
79 Bacterial nanocellulose (BNC) is a bio-polymer non-soluble in aqueous solutions, with high
80 mechanical properties, and thermally resistant. Furthermore, BNC is produced more
81 efficiently through new culture media [26]. Studies show that nanofibers act as bridges over
82 cracks creating reinforcement mechanisms, which prevents crack propagation at the nano
83 level [27,28]. Overall, these properties make this material to be considered as an admixture
84 for cement-based materials [29,30], including in the oil and gas industry [30,31].

There is currently limited information on the effects of bacterial nanocellulose on cement [28,32], and there are no studies on carbonating this cement under supercritical conditions. Recently, authors have utilized BNC as an additive. They observed an improvement in mechanical strength, hydration degree, and thermomechanical properties of cement samples [33]. Therefore, the study of bacterial nanocellulose as an additive for oil well class G cement is a promising alternative to improve cement performance in petroleum engineering applications, especially in the context of geological storage of CO2.

The present work aims to study the porous structure and mechanical properties of cement modified with bacterial nanocellulose after carbonation under supercritical CO_2 conditions similar to geological storage of CO_2. The determination of the temperature and pressure to be used was based on literature, and the fact that carbonation was carried out under the most extreme conditions that could be obtained in the laboratory. Specimens with BNC addition were cured for 28 days at 20°C and then subjected to supercritical CO_2 in an environment at 20 MPa of pressure with a temperature of 90 °C. These conditions are to be expected in deep wells and several authors have worked with similar conditions [9]. Mercury intrusion porosimetry (MIP), X-ray diffraction (XRD), and uniaxial compressive strength (UCS) tests were performed on the carbonated samples. The results of this experimental program are presented and discussed hereafter. Scarce information exists on the subject, so this study allows to expand the current knowledge on the use of this type of additives.

2. Materials and methods

2.1. Materials

The clinker and calcium sulfate were dosed to satisfy the chemical requirements of the American Petroleum Institute (API) Standard 10A for class G oil well cement [34]. The initial chemical composition obtained by X-ray fluorescence (XRF) show 62.39% of CaO, 21.23% of SiO_2, 2.22% of MgO, 3.84% of Al_2O_3, 5.07% of Fe_2O_3, 2.04% of SO_3, and 0.64% of total alkali equivalent.

Bacterial nanocellulose (BNC) is a membrane with fiber diameters between 20 and 50 nm and lengths of 1 μm [26], it differs from other polymers by not having free macromolecules, but is formed by micrometric fibers with nanometric thickness. These fibers have a high mechanical strength necessary to improve the properties of cement [35]. The BNC membranes are approximately 98% water and 2% bacterial nanocellulose. The dispersion method used was ultrasound on previously cut and wet-grinded BNC membranes. Its treatment to obtain an adequate additive for cement requires several steps described in previous works [33]. The final mix of water and BNC contains 0.46% of BNC by mass, and the rest is distilled water. This additive is added to the cement mixture taking into account the already added water.

2.2. Samples preparation

Samples were prepared according to the American Petroleum Institute Standard 10A [34], with a water to cement ratio of 0.44. Three types of mixtures were prepared; Portland cement (PC), cement with the addition of 0.05% BNC (BNC05), and cement with the addition of 0.15% BNC (BNC15). The slurry was poured into 38 mm diameter, 76 mm high cylindrical molds and compacted 27 times in two layers with a puddling rod. The samples were cured for 24 hours in a 20 °C batch and unmolded. After demolding, they were kept under lime-saturated water for 28 days.

2.3. Supercritical CO_2 testing conditions

The carbonation tests were carried out in a titanium vessel of 16 cm in diameter and 20 cm high under static conditions. PC and BNC-modified cement samples were carbonated under wet supercritical CO_2 at 20 MPa and 90 °C, for 30 days and 120 days. Before carbonation, the container with the samples underwater was placed inside a vacuum vessel to remove the air bubbles possibly trapped inside the samples.

The saturated specimens were identified, measured, weighed, and placed on a container grid. A thin water layer was poured at the bottom of the vessel for maintaining humidity (500 ml). The grid was placed inside the cell, avoiding contact between the samples and water layer. The cell was then sealed and connected to the CO_2 pressure line. CO_2

pressure was increased to 8 MPa. The temperature was brought to 90° with the heating system and the pressure regulated at 20 MPa with the leak valve, removing the remaining air on the top of the vessel. This were the initial conditions for the test in static conditions. The ratio of sample volume/vessel volume was 0.38, and the ratio of sample volume/CO_2 volume was 0.79. A diagram of the carbonation system is presented in Fig. 1. After carbonation, the samples were weighed, and photographed. The pH level of the remaining water inside the cell was measured after carbonation.

In the first stage, a total of 18 samples were carbonated for 30 days, of which 6 were Portland Cement (PC), 6 had bacterial nanocellulose content of 0.05% (BNC05), and 6 of 0.15% (BNC15). In the second stage, another group of 18 samples (6 PC; 6 BNC05 and 6 BNC15) were carbonated for 120 days.

After carbonation, three samples of each BNC percentage were used for compressive strength tests, while other samples were cut radially and longitudinally to observe the penetration depth for the different cement types. The remaining cut pieces were used to perform porosimetry tests. These were taken at the middle of each sample, either at the core or near the outer surface.

2.4. Mercury intrusion porosimetry (MIP)

MIP allows to characterize the pore structure of a sample in terms of porosity and pore size distribution (PSD). The basic assumption to interpret MIP data is that pores are cylindrical and interconnected, thus allowing a simple calculation through the Jurin or Washburn equation:

$$\mathrm{p} = \frac{4\Upsilon\cos(\theta)}{d} \quad (5)$$

where Υ = mercury surface tension = 0.485 N/m, θ = mercury contact angle = 130°, p = mercury pressure, d = pore diameter [36].

Eq. 5 permits the determination of the pore entry diameter for each pressure step applied.

165 According to the amount of mercury that penetrated the sample, it is possible to calculate
166 capillary porosity and the PSD. However, the technique does not allow the characterization
167 of isolated pores or pore sizes less than 0.010 μm [37].
168 Before the MIP tests, the samples were freeze-dried. This method was performed by
169 immersing the 1 cm-side cubic samples in liquid nitrogen for 5 minutes, lowering the
170 pressure, and vacuuming for 24 hours (more details are available in [38]). Samples were
171 then kept sealed in containers with silica-gel to prevent rehydration until the MIP test was
172 performed. The equipment utilized was a Micromeritics AutoPore IV 9500 with a maximum
173 pressure of 230 MPa. All non-carbonated MIP samples were taken from a representative
174 zone of the 28 days cured samples (NC). In the carbonated cement case, samples were
175 taken from the core (Int) and near the outer rim (Ext). Two tests were performed on these
176 same zones to analyze repeatability.
177 The list of tests carried out is given in Table 1. The samples reference is: cement type (PC,
178 BNC05, or BNC15), days of carbonation (30 or 120), and location MIP sample (Int or Ext).
179 If it was obtained from the interior or near the exterior of the cylindrical sample.
180 *2.5. X-ray diffraction (XRD)*
181 XRD analysis was performed on a Philips 3020 diffractometer using CuKα radiation with a
182 Ni-filter (35 kV, 40 mA). Scanning was performed between 3° and 70° 2θ, with a step of
183 0.04° and a count time of 2 s/step. No monochromator was used, and openings were 1°
184 for divergence, 0.2° for the reception, and 1° for dispersion. The identification of the mineral
185 phases in the material was performed using the X'Pert High Score program. The
186 procedures described by Moore and Reynolds [39] were followed to identification, while
187 quantification was based on the work of Biscaye [40]. The samples analyzed were taken
188 from non-carbonated specimens (NC) and after 120 days of carbonation. For carbonated
189 specimens, samples were obtained from the interior (120Int) and near the exposed edge
190 (120Ext).
191 *2.6. Uniaxial compression test (UCS).*

192 The uniaxial compression test was performed on a 100 kN testing machine with a 0.5
193 mm/min velocity rate. Vertical displacement and applied force were monitored during the
194 compression tests. The compressive strength and Young's modulus were calculated for all
195 samples. The averages of strength values and Young's modulus were calculated from 3
196 tested cylindrical samples.
197

198 ## 3. Results and discussion

199 Carbonation conditions are critical to obtaining more or less penetration. There have been
200 reports on how carbonation effects are affected by temperature or pressure variations by
201 maintaining one of these parameters constant [41]. It was shown that, by increasing
202 pressure and keeping the temperature constant, the penetration depth was lower and the
203 compressive strength was higher. On the other hand, when the pressure was maintained
204 constant and the temperature increased, cement was more affected with a larger
205 penetration depth and a further reduction in compressive strength.
206 After 120 days of carbonation, the specimens have not been completely carbonated.
207 Therefore, the results shown here are of a cement not totally carbonated in the interior. The
208 carbonation conditions of the current work are similar to Barlet-Gouedard and Fabbri
209 [17,42], where larger penetrations or complete penetration have been observed after 30
210 days of carbonation. However, the carbonation effect in our samples is different, similar to
211 the small penetrations observed by Kutchko and Gu [12,43]. The slow advancement rate
212 in our samples is explained by their low capillary porosity (19%) compared to the
213 aforementioned authors [17,42] (33% - 41%).
214 The samples have a thin brown outer ring, and a thinner darker brown ring was observed
215 surrounding the interior part of the brown ring in some samples. The change in color in the
216 altered zones might result from the release of Fe^{3+} ions, which react chemically and form
217 iron hydroxides [44]. This comes from the fact that the brownmillerite begins to carbonate,
218 due to a decrease in the amount of crystals in the XRD results in Table 3.

As shown in Fig. 2, the degraded zone has a slow penetration rate, and no change can be seen at the core of the specimens. However, in the top part, a substantial penetration is observed. BNC05 cement was less degraded than PC. Lower amounts of calcium hydroxides characterize this zone and a lower Ca/Si ratio in the C-S-H structure [45].

The top degraded zone observed in Fig. 2 might result from sedimentation during the cement setting, which leaves a more porous area at the top of the sample. This zone measured with caliper penetrates 8.7 mm inwards from the top of the PC sample, while a value of 5.6 mm is measured for BNC05. The porosity of BNC05 in the top part was lower than for PC, due to BNC's ability to diminish cement sedimentation by reducing the free water content [33], thus allowing this part to have more cement hydrates and less porosity. Bacterial nanocellulose is known for enhancing the creation of more cement hydrates for prolonged curing times [46].

After carbonation, the fluid pH was reduced from 13 to 7, similar to studies of Barlet-Gouédard [47]. Unfortunately, the pH could not be measured during the carbonation test. In fact, the pH during the carbonation process could be reduced to 2.9 [12] or 3.2 [48], depending on CO_2 solubility in water. According to Duan and Carey's model [48,49], the solubility of CO_2 in our experiment was 1.1 mol/kg.

3.1 Density variation

Table 2 shows the density variation of samples over the 30 and 120 days of carbonation. These values are the averages of all the samples tested, and the deviation does not exceed 2% of the averages.

PC increases its bulk density by 1.4% and 2.5% at 30 and 120 days, respectively. BNC05 was the lightest compared to the other two cement types and showed an increase of its density by 1.5% and 2%, respectively. BNC15 had the greatest initial densities and increased 1.3% and 3.6% at 30 and 120 days, respectively.

The stoichiometric relation between the solid phases CH and $CaCO_3$ is one. As the density of CH is 2.23 g/cm^3, and $CaCO_3$ is 2.71 g/cm^3 (or 2.93 g/cm^3 for aragonite or 2.54 g/cm^3 for vaterite), bulk density will increase. C-S-H is an amorphous material that have different

247 phases with different densities, ranging from 2.6 g/cm^3 to 2.86 g/cm^3 [50]. The C-S-H
248 chemical balance of Eq. 4 indicates that density will also increase due to the formation of
249 $CaCO_3$, with a relation of 1.7 mol of $CaCO_3$ per 1 mol of C-S-H carbonated. Less variation
250 in density is an indicator of a lower degree of carbonation.

251 3.2 *MIP: non-carbonated cement*

252 MIP tests are shown in Fig. 3, Fig. 4, and Fig. 5. Adding bacterial nanocellulose led to lower
253 porosity, and the characteristic pore size peak shifted to smaller pores (from 0.050 to 0.045
254 μm). Cellulose nanocrystals have been reported to reduce porosity in cement for pores
255 smaller than 0.100 μm [51]. The hydrophilic properties of bacterial nanocellulose induce
256 the precipitation of larger quantities of hydration products during hydration [33,52], thus
257 accumulating more of them in the pores previously filled with water [53]. Furthermore, the
258 fibers of the bacterial nanocellulose have substantial mechanical strength characteristics
259 [35], which during cement shrinkage decrease the probability of having micro-cracks [54].
260 PC has an average of 19% capillary porosity, while BNC05 has an average of 12% and
261 BNC15 of 16% (blue dots). Nanocellulose distribution within the samples is crucial in
262 obtaining homogeneous properties, but it cannot be easily measured. An uneven
263 distribution can lead to scattering in measurements [55]. The ultrasonic scrubber allowed
264 us to have a better distribution of BNC in the mix [56]. However, in Fig. 6, MIP results for
265 the non-carbonated cement with bacterial nanocellulose show some scatter certainly due
266 to heterogeneity.

267 *3.3 MIP: Carbonated cement paste*

268 The variation in the shape of MIP curves means that the characteristic peak of PSD tends
269 to disappear, and smaller pores (less than 0.010 μm) begin to appear after 30 days. As
270 carbonation continues towards 120 days, the smaller pores are continuously reduced.
271 While this was happening, the CH and C-S-H were being dissolved, thus increasing the
272 smallest pores at 0.020 μm.

273 In Fig. 3 to Fig. 5 after 30-days of carbonation, PC, BNC05, and BNC15 samples show an
274 increase in pores' population having a diameter close to 0.100 μm. That population was

quasi inexistent in pre-carbonated samples. Some authors have confirmed the occurrence of nano-cracks and micro-cracks after carbonation shrinkage [57], probably induced by calcite crystallization in pores [58]. However, this specific increment of the pore volume could be due to CH dissolution or C-S-H decalcification. In fact, studies on the dissolution of CH and C-S-H indicate a similar porosity increment at 0.100 μm [59]. Once the pH drops in the pore solution due to the CH leaching, the dissolution of ettringite (pH < 10.7) and C-S-H (pH < 10.5 or 8.8 depending on the study [60]) will begin.

Regardless of this pore size growth of 0.100 μm in Fig. 3 to Fig. 5 after 30 days of carbonation, these pore sizes of 0.100 μm disappear in samples carbonated for 120 days. C-S-H decalcification is the one that produces more $CaCO_3$ that further clogs the pores after 120 days of carbonation, according to Morandeau studies [10]. As samples were not underwater, dissolved ions could not be released out of the specimens. Therefore, the $CaCO_3$ precipitation has been refilling these carbonation-induced cracks from the hydrated material of the core, and blocking further carbonation inwards. This remains to be confirmed by analyzing SEM images.

PC results in Fig. 7 show a porosity decrease at the cement core (blue dots), suggesting that chemical reactions of carbonation have reached this point. The carbonation process becomes clearer here by looking at the PSD variation in Fig. 8. Indeed, MIP results suggest that carbonation exists all over the sample, at a relatively slow rate at the center and a faster one near the outer rim, where a carbonation front can visually be identified. This was observed first by Rimmelé [18], who reported that CH depletion and $CaCO_3$ precipitation occurred at the cement core, ahead of the carbonation front. Later, Adeoye [61] noted that the Vickers hardness increases throughout the material after carbonation.

As in non-carbonated samples, we can observe a shift of the characteristic peak at the core of carbonated samples. The characteristic peak is centered on 0.015 μm for BNC and 0.020 μm for PC. This shows that the effects of nanocellulose remain during cement carbonation, maintaining its characteristic peak at lower values than for PC.

According to Kutchko [12], the carbonation causes a decrease in CH amount at the inner part of cement, and a decrease in porosity over the carbonate barrier. Although $CaCO_3$ precipitation is seen, a large number of pores smaller than 0.020 μm are observed.

3.4 X-ray diffraction (XRD)

Fig. 9 shows the XRD patterns of PC and BNC15, while Table 3 indicates the relative percentage of the crystalline phases**.** The increase in the amount of portlandite and decrease in browmillerite in samples before carbonation reinforces the results obtained in previous studies showing that BNC increases the degree of cement hydration [33]. XRD curves are similar to other types of G-cements [62], showing similar crystals. The lack of ettringite and monosulfoaluminates is due to the low content of C_3A and gypsum in cement [63,64]. Katoite and silicious hydrogarnet can be form from C_2S and C_4AF and they have a similar chemical formula depending on fluid condition, sulfate activity, and temperature. Here, both are listed as katoite in Table 3. Additionally, the lack of crystals related to C-S-H is due to the insufficient intensity of reflection of this amorphous material [65].

The post-carbonation XRD results on the exposed surface indicate almost complete carbonation. A large amount of aragonite in this area denotes higher chemical instability due to its high solubility. The core is less affected by carbonation, but the percentages of minerals have changed. The increase in katoite is probably a combination of temperature effect during carbonation, as this material is more stable at higher temperatures, and C_4AF hydration. In fact, katoite was found to increase significantly upon hydration of C_4AF.

BNC15 shows a decrease in portlandite, suggesting that CH dissolution has started. However, this is not observed in PC cement. Some aragonite traces are detected at the core of the PC sample. Carbonation and/or hydration during the test produced a change in the amount of katoite and brownmillerite, while portlandite and carbonates do not appear to have changed. This seems to indicate that the core did not undergo carbonation, differing from the MIP and total porosity results.

3.5 Uniaxial compression tests (UCS)

329 In supercritical conditions, some authors have reported an increment in compressive
330 strength [41,66], while more recent researchers report a decrease in mechanical
331 performance [42,67,68]. This contradiction stems from the different hydration conditions
332 before carbonation [69] and the subsequent carbonation conditions [41]. For the same
333 water/cement ratio before the carbonation test, the advance of carbonation is dependent
334 on the hydration level. A well-hydrated cement will probably only experience mechanical
335 degradation, while an early-carbonated cement specimen will also show the effects of
336 ongoing hydration [70].
337 In Fig. 10, supercritical carbonation is adversely affecting the mechanical performance.
338 Several reasons can explain this: micro-cracks due to pressure variation in the carbonation
339 cell, the high porosity and softening of the outer layer due to $CaCO_3$ dissolution [71], the
340 degradation of C-S-H [72], possible cracks due to increased crystallization stresses of
341 $CaCO_3$ in the pores [42,73], or the preferential paths of the cracks through the different
342 interfaces of the rings of the carbonated material [42]. Pore crystallisation is the overgrowth
343 of $CaCO_3$ and begins to generate tensile stresses from within the pore.
344 C-S-H decalcification is mainly responsible for the strength loss during carbonation [74],
345 and Young's modulus in leached zones can decrease up to 80% [75]. It was observed by
346 Hidalgo [76] that CH is depleted rapidly and carbonation products surround the remains.
347 The discontinuities between the different rings of the carbonation zones generate stress
348 concentrations and can initiate failures during compression. Some of our samples broke
349 parallel to the applied force and near the rim, as observed by other authors [42].
350 $CaCO_3$ crystallization can produce tensile stresses around the pores [77,78]. However, it
351 is difficult to see this after the carbonation process. Once the confinement pressure is
352 removed, the pore increases its volume again, and the crystals can be re-solubilized in the
353 fluid. A work carried out by Lesti highlighted the problems of pore crystallization [73]. In that
354 report, even though the carbonation front did not advance deeply, cracks were visually
355 appreciated, which enhanced the failure probability of the sample.

Nanocellulose has been reported incrementing mechanical properties when added to cement mixtures [28,54,79]. Results in this work show an initial increment in strength due to the addition of bacterial nanocellulose before carbonation. They were also less affected by carbonation. After 120 days of carbonation, the PC strength is 36 MPa, while BNC05 and BNC15 are 48 MPa and 42 MPa. Young's modulus was also affected in PC to a value of 16.5 GPa, while BNC and BNC15 had 22 and 21 GPa. The increased level of cement hydration from the hydrophilic characteristics of BNC probably reduced the progression of carbonation. Indeed, the lower capillary porosity due to the higher degree of hydration slows down the diffusion rate [20].

3.6 Porosity development in time

Fig. 11 shows the pore size diameter variation at a material point near the external surface of PC from the initial state (no carbonation) to 120 days of carbonation where: Time 1 is before carbonation, Time 2 is 30 days of carbonation and Time 3 is 120 days of carbonation.

The corresponding porosities are 19%, 14% and 5% for PC. All of our cement types behave in this manner with their corresponding capillary porosities. As seen before, the $CaCO_3$ growth in pores shifts the characteristic peak from 0.050 μm to 0.010 μm after 30 days. At this time, an increment of 0.100 μm pores is observed. After 120 days of carbonation, C-S-H depletion continues but towards smaller pores, and $CaCO_3$ continues growing inside the smallest pores. At this point, no cracks are observed, the ones that appeared previously having been filled by $CaCO_3$ precipitation.

4. Conclusions

A supercritical carbonation test was performed on cement modified with bacterial nanocellulose for 30 and 120 days. Density variation was measured. Capillary porosity was measured by mercury intrusion porosimetry on different zones. X-ray diffraction was used to characterize the crystalline phases. Compressive strength values and Young's modulus were calculated from uniaxial compressive strength tests. Results are summarized below:

- Density has increased in all samples, but cement with 0.05% of BNC was the lightest. A substantial degraded zone was seen at the top of the samples, but cement was less damaged radially.
- A clear reduction in capillary porosity was noted radially over the exterior of the samples during the 120 days of carbonation.
- At the core, capillary porosity was reduced in PC and BNC15 samples but not for BNC05. The pore distribution from MIP results indicates the existence of 0.100 μm microcracks after 30 days of carbonation, but they disappear after 120 days of carbonation.
- XRD results show more crystalline phases of hydrated cement in the BNC samples before carbonation. A large amount of aragonite in the outer rim indicate that dissolution of the $CaCO_3$ minerals can take place if external conditions allowed it.
- Carbonation generates a reduction in the mechanical strength and Young's modulus of all samples. Non-modified cement shows a continuous decline in strength, while samples with BNC maintain the same strength from 30 to 120 days. Samples with BNC show higher values of their mechanical properties in absolute and relative terms before and after the carbonation process.
- Cement with 0.05% of bacterial nanocellulose visually presents a lesser degraded zone and is not affected at the center of the sample as the other mixtures. The average ultimate strength of this cement is 48 MPa, 33% higher than the unmodified cement, which was 36 MPa. However, there are no significant variations in porosity and XRD results.

Acknowledgments

The first author gratefully acknowledges the fellowship granted by the National Scientific and Technical Research Council of Argentina (CONICET) and to the EIFFEL fellowship program of Excellence granted by the Ministère de l'Europe et des Affaires étrangères of France. The authors acknowledged the financial support of the European Union's Horizon 2020 research and innovation program under the Grant Agreement N° 101007851

(H2020 MSCA-RISE 2020 Project DISCO2-STORE), the Universidad Nacional de la Patagonia San Juan Bosco -Project UNPSJB PI1614 80020190200006 IP, Res. R/9Nº207-2020 CRD1365 FI004/ 17-, the Agency of Scientific and Technological Promotion from the Argentine Republic. (Projects PICT 2016–4543, PICT 0843 2016), and the Institutional project ITPN PUE 0034 (CONICET).

References

[1] J.M. Belbute, A.M. Pereira, ARFIMA Reference Forecasts for Worldwide CO_2 Emissions and the Need for Large and Frontloaded Decarbonization Policies, Lisboa, 2019.

[2] H. Herzog, D. Golomb, Carbon Capture and Storage from Fossil Fuel Use, Encycl. Energy. 1 (2004) 277–287. https://doi.org/10.1016/b0-12-176480-x/00422-8.

[3] D.A. Voormeij, G.J. Simandl, Geological, ocean, and mineral CO_2 sequestration options: A technical review, Geosci. Canada. 31 (2004) 11–22.

[4] Philip Ringrose, How to Store CO_2 Underground: Insights from early-mover CCS Projects, Springer, 2020.

[5] K. Michael, A. Golab, V. Shulakova, J. Ennis-king, G. Allinson, S. Sharma, T. Aiken, Geological storage of CO 2 in saline aquifers — A review of the experience from existing storage operations, Int. J. Greenh. Gas Control. 4 (2010) 659–667. https://doi.org/10.1016/j.ijggc.2009.12.011.

[6] S. Bachu, D. Bonijoly, J. Bradshaw, R. Burruss, S. Holloway, N.P. Christensen, O.M. Mathiassen, CO_2 storage capacity estimation: Methodology and gaps, Int. J. Greenh. Gas Control. 1 (2007) 430–443. https://doi.org/10.1016/S1750-5836(07)00086-2.

[7] S.E. Gasda, S. Bachu, M.A. Celia, Spatial characterization of the location of potentially leaky wells penetrating a deep saline aquifer in a mature sedimentary basin, Environ. Geol. 46 (2004) 707–720. https://doi.org/10.1007/s00254-004-1073-5.

[8] M. Bai, Z. Zhang, X. Fu, A review on well integrity issues for CO_2 geological storage and enhanced gas recovery, Renew. Sustain. Energy Rev. 59 (2016) 920–926. https://doi.org/10.1016/j.rser.2016.01.043.

[9] M. Bagheri, S.M. Shariatipour, E. Ganjian, A review of oil well cement alteration in CO_2-rich environments, Constr. Build. Mater. 186 (2018) 946–968. https://doi.org/10.1016/j.conbuildmat.2018.07.250.

[10] A. Morandeau, M. Thiéry, P. Dangla, Investigation of the carbonation mechanism of CH and C-S-H in terms of kinetics, microstructure changes and moisture properties, Cem. Concr. Res. 56 (2014) 153–170. https://doi.org/10.1016/j.cemconres.2013.11.015.

[11] V. Shah, K. Scrivener, B. Bhattacharjee, S. Bishnoi, Changes in microstructure characteristics of cement paste on carbonation, Cem. Concr. Res. 109 (2018) 184–197. https://doi.org/10.1016/j.cemconres.2018.04.016.

[12] B.G. Kutchko, B.R. Strazisar, D.A. Dzombak, G. V. Lowry, N. Thauiow, Degradation of well cement by CO_2 under geologic sequestration conditions, Environ. Sci. Technol. 41 (2007) 4787–4792. https://doi.org/10.1021/es062828c.

[13] Y.J. Jeong, K.S. Youm, T.S. Yun, Effect of nano-silica and curing conditions on the reaction rate of class G well cement exposed to geological CO_2-sequestration conditions, Cem. Concr. Res. 109 (2018) 208–216. https://doi.org/10.1016/j.cemconres.2018.05.001.

[14] N. Neuville, E. Lécolier, G. Aouad, A. Rivereau, D. Damidot, Effect of curing conditions on oilwell cement paste behaviour during leaching: Experimental and modelling approaches, Comptes Rendus Chim. 12 (2009) 511–520. https://doi.org/10.1016/j.crci.2008.06.006.

[15] B.L. d. S. Costa, J.C. d. O. Freitas, D.M. d. A. Melo, R.G. d. S. Araujo, Y.H. d. Oliveira, C.A. Simão, Evaluation of density influence on resistance to carbonation process in oil well cement slurries, Constr. Build. Mater. 197 (2019) 331–338. https://doi.org/10.1016/j.conbuildmat.2018.11.232.

[16] D. Buhmann, W. Dreybrodt, The kinetics of calcite dissolution and precipitation in geologically relevant situations of karst areas. 2. Closed system, Chem. Geol. 53 (1985) 109–124. https://doi.org/10.1016/0009-2541(85)90024-5.

[17] V. Barlet-Gouedard, G. Rimmelé, B. Goffé, O. Porcherie, Well Technologies for CO 2 Geological Storage : CO 2 -Resistant Cement, SPE Int. 62 (2007) 325–334. https://doi.org/10.2516/ogst.

[18] G. Rimmelé, V. Barlet-Gouédard, O. Porcherie, B. Goffé, F. Brunet, Heterogeneous porosity distribution in Portland cement exposed to CO_2-rich fluids, Cem. Concr. Res. 38 (2008) 1038–1048. https://doi.org/10.1016/j.cemconres.2008.03.022.

[19] S. Ghabezloo, J. Sulem, J. Saint-Marc, Evaluation of a permeability-porosity relationship in a low-permeability creeping material using a single transient test, Int. J. Rock Mech. Min. Sci. 46 (2009) 761–768. https://doi.org/10.1016/j.ijrmms.2008.10.003.

[20] M. Mainguy, modeles de diffusion non-lineaires en milieux poreux. Applications a la dissolution et au sechage des materiaux cimentaires, 1999.

[21] C. Gómez Hoyos, E. Cristia, A. Vázquez, Effect of cellulose microcrystalline particles on properties of cement based composites, Mater. Des. 51 (2013) 810–818. https://doi.org/10.1016/j.matdes.2013.04.060.

[22] R. Mejdoub, H. Hammi, J.J. Suñol, M. Khitouni, S. Boufi, Nanofibrillated cellulose as nanoreinforcement in Portland cement : Thermal , mechanical and microstructural properties, J. Compos. Mater. 51 (2017) 2491–2503. https://doi.org/10.1177/0021998316672090.

[23] J.C. Barría, D.G. Manzanal, C.M. Martín, T. Piqué, J.M. Pereira, Cement-rock interface subjected to $SCCO_2$, in: Rock Mech. Nat. Resour. Infrastruct. Dev. Proc. 14th Int. Congr. Rock Mech. Rock Eng. ISRM 2019, 2020: pp. 3196–3203.

[24] J.C. Barría, D. Manzanal, J.M. Pereira, S. Ghabezloo, CO_2 geological storage: Microstructure and mechanical behavior of cement modified with a biopolymer

after carbonation, E3S Web Conf. 205 (2020). https://doi.org/10.1051/e3sconf/202020502007.

[25] J.N. de Paula, J.M. Calixto, L.O. Ladeira, P. Ludvig, T.C.C. Souza, J.M. Rocha, A.A.V. de Melo, Mechanical and rheological behavior of oil-well cement slurries produced with clinker containing carbon nanotubes, J. Pet. Sci. Eng. 122 (2014) 274–279. https://doi.org/10.1016/j.petrol.2014.07.020.

[26] P. Cerrutti, P. Roldán, R.M. García, M.A. Galvagno, A. Vázquez, M.L. Foresti, Production of bacterial nanocellulose from wine industry residues: Importance of fermentation time on pellicle characteristics, J. Appl. Polym. Sci. 133 (2016). https://doi.org/10.1002/app.43109.

[27] M.S. El-Feky, P. Youssef, A.M. El-Tair, S. Ibrahim, M. Serag, Effect of nano silica addition on enhancing the performance of cement composites reinforced with nano cellulose fibers, AIMS Mater. Sci. 6 (2019) 864–883. https://doi.org/10.3934/matersci.2019.6.864.

[28] M.A. Akhlaghi, R. Bagherpour, H. Kalhori, Application of bacterial nanocellulose fibers as reinforcement in cement composites, Constr. Build. Mater. 241 (2020) 118061. https://doi.org/10.1016/j.conbuildmat.2020.118061.

[29] A. Vazquez, M.L. Foresti, P. Cerrutti, M. Galvagno, Bacterial Cellulose from Simple and Low Cost Production Media by Gluconacetobacter xylinus, J. Polym. Environ. 21 (2013) 545–554. https://doi.org/10.1007/s10924-012-0541-3.

[30] A. Vázquez, T.M. Pique, Biobased Additives in Oilwell Cement, in: Ind. Appl. Renew. Biomass Prod. Past, Present Futur., 2017: pp. 179–198. https://doi.org/10.1007/978-3-319-61288-1.

[31] M. Panchuk, L. Shlapak, A. Panchuk, M. Szkodo, W. Kiełczy, Perspectives of use of nanocellulose in oil and gas industry, J. Hydrocarb. Power Eng. 3 (2016) 79–84.

[32] F. Mohammadkazemi, R. Aguiar, N. Cordeiro, Improvement of bagasse fiber–cement composites by addition of bacterial nanocellulose: an inverse gas chromatography study, Cellulose. 24 (2017) 1803–1814.

https://doi.org/10.1007/s10570-017-1210-4.

[33] J.C. Barría, A. Vázquez, J.M. Pereira, D. Manzanal, Effect of bacterial nanocellulose on the fresh and hardened states of oil well cement, J. Pet. Sci. Eng. 199 (2021). https://doi.org/10.1016/j.petrol.2020.108259.

[34] API Specification 10A, Specification for Cements and Materials for Well Cementing, Twenty-Fif, Northwest Washington, DC, 2019. https://www.techstreet.com/standards/api-spec-10a?product_id=2038411.

[35] P. Gatenholm, D. Klemm, Bacterial Nanocellulose as a Reneable Material for Biomedical Applications, MRS Bull. 35 (2010) 208–213. https://doi.org/10.1080/15440478.2018.1439426.

[36] S. Diamond, Pore Size Distributions in Clays, Clays Clay Miner. 18 (1970) 7–23. https://doi.org/10.1346/ccmn.1970.0180103.

[37] M.B. Pinson, E. Masoero, P.A. Bonnaud, H. Manzano, Q. Ji, S. Yip, J.J. Thomas, M.Z. Bazant, K.J. Van Vliet, H.M. Jennings, Hysteresis from multiscale porosity: Modeling water sorption and shrinkage in cement paste, Phys. Rev. Appl. 3 (2015) 1–17. https://doi.org/10.1103/PhysRevApplied.3.064009.

[38] P. Delage, D. Tessier, M. Marcel-Audiguier, Use of the Cryoscan apparatus for observation of freeze-fractured planes of a sensitive Quebec clay in scanning electron microscopy, Can. Geotech. J. 19 (1982) 111–114. https://doi.org/10.1139/t82-011.

[39] D.M. Moore, R.C. Reynolds Jr, X-Ray Diffraction and the Identification and Analysis of Clay Minerals-Oxford University Press., 1989.

[40] P.E. Biscaye, Geological Society of America Bulletin Mineralogy and Sedimentation of Recent Deep-Sea Clay in the Atlantic Ocean and Adjacent Seas and Oceans, Geol. Soc. Am. Bulletim. 76 (1965) 803–832. https://doi.org/10.1130/0016-7606(1965)76.

[41] A. Sauki, S. Irawan, Effects of Pressure and Temperature on Well Cement Degradation by Supercritical CO 2, Int. J. Eng. Technol. IJET-IJENS. 10 (2010)

53–61.

[42] A. Fabbri, J. Corvisier, A. Schubnel, F. Brunet, B. Goffé, G. Rimmele, V. Barlet-Gouédard, Effect of carbonation on the hydro-mechanical properties of Portland cements, Cem. Concr. Res. 39 (2009) 1156–1163. https://doi.org/10.1016/j.cemconres.2009.07.028.

[43] T. Gu, X. Guo, Z. Li, X. Cheng, X. Fan, A. Korayem, W.H. Duan, Coupled effect of CO_2 attack and tensile stress on well cement under CO_2 storage conditions, Constr. Build. Mater. 130 (2017) 92–102. https://doi.org/10.1016/j.conbuildmat.2016.10.117.

[44] J.W. Carey, M. Wigand, S.J. Chipera, G. WoldeGabriel, R. Pawar, P.C. Lichtner, S.C. Wehner, M.A. Raines, G.D. Guthrie, Analysis and performance of oil well cement with 30 years of CO_2 exposure from the SACROC Unit, West Texas, USA, Int. J. Greenh. Gas Control. 1 (2007) 75–85. https://doi.org/10.1016/S1750-5836(06)00004-1.

[45] H.B. Jung, W. Um, Experimental study of potential wellbore cement carbonation by various phases of carbon dioxide during geologic carbon sequestration, Appl. Geochemistry. 35 (2013) 161–172. https://doi.org/10.1016/j.apgeochem.2013.04.007.

[46] X. Sun, Q. Wu, S. Lee, Y. Qing, Y. Wu, Cellulose Nanofibers as a Modifier for Rheology, Curing and Mechanical Performance of Oil Well Cement, Sci. Rep. 6 (2016) 1–9. https://doi.org/10.1038/srep31654.

[47] V. Barlet-Gouédard, G. Rimmelé, B. Goffé, O. Porcherie, Well Technologies for CO_2 Geological Storage: CO_2 -Resistant Cement, Oil Gas Sci. Technol. - Rev. l'IFP. 62 (2007) 325–334. https://doi.org/10.2516/ogst:2007027.

[48] J.W. Carey, Geochemistry of Wellbore Integrity in CO_2 Sequestration: Portland Cement-Steel-Brine-CO_2 Interactions, Rev. Mineral. Geochemistry. 77 (2013) 505–539. https://doi.org/10.2138/rmg.2013.77.15.

[49] Z. Duan, R. Sun, An improved model calculating CO_2 solubility in pure water and

578 aqueous NaCl solutions from 273 to 533 K and from 0 to 2000 bar, Chem. Geol.
579 193 (2003) 257–271. https://doi.org/10.1016/S0009-2541(02)00263-2.
580 [50] J.J. Thomas, H.M. Jennings, A.J. Allen, Relationships between composition and
581 density of tobermorite jennite CSH, J. Phys. Chem. C. 114 (2010) 7594–7601.
582 [51] M.R. Dousti, Y. Boluk, V. Bindiganavile, The effect of cellulose nanocrystal (CNC)
583 particles on the porosity and strength development in oil well cement paste,
584 Constr. Build. Mater. 205 (2019) 456–462.
585 https://doi.org/10.1016/j.conbuildmat.2019.01.073.
586 [52] Y. Cao, P. Zavaterri, J. Youngblood, R. Moon, J. Weiss, The influence of cellulose
587 nanocrystal additions on the performance of cement paste, Cem. Concr. Compos.
588 56 (2015) 73–83. https://doi.org/10.1016/j.cemconcomp.2014.11.008.
589 [53] A. Balea, E. Fuente, A. Blanco, C. Negro, Nanocelluloses: Natural-based materials
590 for fiber- reinforced cement composites. A critical review, Polymers (Basel). 11
591 (2019). https://doi.org/10.3390/polym11030518.
592 [54] O.A. Hisseine, W. Wilson, L. Sorelli, B. Tolnai, A. Tagnit-Hamou, Nanocellulose for
593 improved concrete performance: A macro-to-micro investigation for disclosing the
594 effects of cellulose filaments on strength of cement systems, Constr. Build. Mater.
595 206 (2019) 84–96. https://doi.org/10.1016/j.conbuildmat.2019.02.042.
596 [55] G. Chauve, J. Bras, Industrial Point of View of Nanocellulose Materials and Their
597 Possible Applications, in: 2014: pp. 233–252.
598 https://doi.org/10.1142/9789814566469_0014.
599 [56] V.A. Barbash, O. V. Yaschenko, S. V. Alushkin, A.S. Kondratyuk, O.Y.
600 Posudievsky, V.G. Koshechko, The Effect of Mechanochemical Treatment of the
601 Cellulose on Characteristics of Nanocellulose Films, Nanoscale Res. Lett. 11
602 (2016) 16–23. https://doi.org/10.1186/s11671-016-1632-1.
603 [57] B. Wu, G. Ye, Development of porosity of cement paste blended with
604 supplementary cementitious materials after carbonation, Constr. Build. Mater. 145
605 (2017) 52–61. https://doi.org/10.1016/j.conbuildmat.2017.03.176.

606 [58] D. Manzanal, V. Vallin, J.M. Pereira, A chemo-poromechanical model for
607 well/caprock interface in presence of CO_2, Poromechanics V - Proc. 5th Biot Conf.
608 Poromechanics. (2013) 1470–1477. https://doi.org/10.1061/9780784412992.175.
609 [59] K. Haga, S. Sutou, M. Hironaga, S. Tanaka, S. Nagasaki, Effects of porosity on
610 leaching of Ca from hardened ordinary Portland cement paste, Cem. Concr. Res.
611 35 (2005) 1764–1775. https://doi.org/10.1016/j.cemconres.2004.06.034.
612 [60] M. Alexander, A. Bertron, N. De Belie, Performance of Cement-Based Materials in
613 Aggressive Aqueous Environments, 2013. https://doi.org/10.1007/978-94-007-
614 5413-3.
615 [61] J.T. Adeoye, A.B.R. Ellis, P. Northwest, Application of Engineered Cementitious
616 Composites for Enhanced Wellbore Integrity During Geologic Carbon
617 Sequestration, (2019).
618 [62] S. Bahafid, S. Ghabezloo, M. Duc, P. Faure, J. Sulem, Effect of the hydration
619 temperature on the microstructure of Class G cement: C-S-H composition and
620 density, Cem. Concr. Res. 95 (2017) 270–281.
621 https://doi.org/10.1016/j.cemconres.2017.02.008.
622 [63] L. Black, C. Breen, J. Yarwood, C.S. Deng, J. Phipps, G. Maitland, Hydration of
623 tricalcium aluminate (C3A) in the presence and absence of gypsum - Studied by
624 Raman spectroscopy and X-ray diffraction, J. Mater. Chem. 16 (2006) 1263–1272.
625 https://doi.org/10.1039/b509904h.
626 [64] S. Bahafid, A multi-technique investigation of the effect of hydration temperature
627 on the microstructure and mechanical properties of cement paste, 2017.
628 https://pastel.archives-ouvertes.fr/tel-01980576.
629 [65] R. Melzer, E. Eberhard, Phase identification during early and middle hydration of
630 tricalciumsilicate (Ca3SiO5), Cem. Concr. Res. 19 (1989) 411–422.
631 https://doi.org/10.1016/0008-8846(89)90030-6.
632 [66] R.A. Bruckdorfer, Carbon Dioxide Corrosion in Oilwell Cements, Soc. Pet. Eng.
633 (1986). https://doi.org/10.2118/15176-MS.

[67] M. Lesti, C. Tiemeyer, J. Plank, CO_2stability of Portland cement based well cementing systems for use on carbon capture & storage (CCS) wells, Cem. Concr. Res. 45 (2013) 45–54. https://doi.org/10.1016/j.cemconres.2012.12.001.

[68] B. Xu, B. Yuan, Y. Wang, S. Zeng, Y. Yang, Nanosilica-latex reduction carbonation-induced degradation in cement of CO_2 geological storage wells, J. Nat. Gas Sci. Eng. 65 (2019) 237–247. https://doi.org/10.1016/j.jngse.2019.03.013.

[69] B.L. de S. Costa, J.C. de O. Freitas, P.H.S. Santos, D.M. de A. Melo, R.G. da S. Araujo, Y.H. de Oliveira, Carbonation in oil well Portland cement: Influence of hydration time prior to contact with CO_2, Constr. Build. Mater. 159 (2018) 252–260. https://doi.org/10.1016/j.conbuildmat.2017.10.103.

[70] J.C. Barría, D. Manzanal, P. Cerrutti, J.M. Pereira, Cement with bacterial nanocellulose cured at reservoir temperature: Mechanical performance in the context of CO_2 geological storage, Geomech. Energy Environ. (2021) 15. https://doi.org/10.1016/j.gete.2021.100267.

[71] A. Duguid, G.W. Scherer, Degradation of oilwell cement due to exposure to carbonated brine, Int. J. Greenh. Gas Control. 4 (2010) 546–560. https://doi.org/10.1016/j.ijggc.2009.11.001.

[72] O. Omosebi, H. Maheshwari, R. Ahmed, S. Shah, S. Osisanya, A. Santra, A. Saasen, Investigating temperature effect on degradation of well cement in HPHT carbonic acid environment, J. Nat. Gas Sci. Eng. 26 (2015) 1344–1362. https://doi.org/10.1016/j.jngse.2015.08.018.

[73] M. Lesti, C. Tiemeyer, J. Plank, CO_2 stability of Portland cement based well cementing systems for use on carbon capture & storage (CCS) wells, Cem. Concr. Res. 45 (2013) 45–54. https://doi.org/10.1016/j.cemconres.2012.12.001.

[74] C. Carde, R. François, Modelling the loss of strength and porosity increase due to the leaching of cement pastes, Cem. Concr. Compos. 21 (1999) 181–188. https://doi.org/10.1016/S0958-9465(98)00046-8.

[75] E. Stora, B. Bary, Q.C. He, E. Deville, P. Montarnal, Modelling and simulations of

the chemo-mechanical behaviour of leached cement-based materials: Interactions between damage and leaching, Cem. Concr. Res. 40 (2010) 1226–1236. https://doi.org/10.1016/j.cemconres.2010.04.002.

[76] A. Hidalgo, C. Domingo, C. Garcia, S. Petit, C. Andrade, C. Alonso, Microstructural changes induced in Portland cement-based materials due to natural and supercritical carbonation, J. Mater. Sci. 43 (2008) 3101–3111. https://doi.org/10.1007/s10853-008-2521-5.

[77] A. Fabbri, N. Jacquemet, D.M. Seyedi, A chemo-poromechanical model of oilwell cement carbonation under CO 2 geological storage conditions, Cem. Concr. Res. 42 (2012) 8–19. https://doi.org/10.1016/j.cemconres.2011.07.002.

[78] D. Manzanal, J.M. Pereira, Effects of the presence of CO_2 at the well/caprock interface: Crystallization damage, in: Proc. Int. Conf. Offshore Mech. Arct. Eng. - OMAE, Nantes, 2013: pp. 1–6. https://doi.org/10.1115/OMAE2013-11543.

[79] X. Sun, Q. Wu, J. Zhang, Y. Qing, Y. Wu, S. Lee, Rheology, curing temperature and mechanical performance of oil well cement: Combined effect of cellulose nanofibers and graphene nano-platelets, Mater. Des. 114 (2017) 92–101. https://doi.org/10.1016/j.matdes.2016.10.050.

Table Captions

Table 1. MIP tests

Table 2. Average values of density and mass absorption after carbonation

Table 3. Relative percentage of the crystalline phases before and after exposure

Figure Captions

Fig. 1. Carbonation system

Fig. 2. PC (Left longitudinal and top radial samples) and BNC05 (right longitudinal and inferior radial) samples after 120 days of carbonation

Fig. 3. Cumulative intrusion volume and PSD of PC

Fig. 4. Cumulative intrusion volume and PSD of BNC05

690 **Fig. 5.** Cumulative intrusion volume and PSD of BNC15

691 **Fig. 6.** Capillary porosity of non-carbonated samples and 30-days carbonated samples
692 (PC, BNC05 and BNC15)

693 **Fig. 7.** Capillary porosities at the core (Interior) and near the exposed surface (Exterior) of
694 samples after 120-days of carbonation (PC, BNC05 and BNC15).

695 **Fig. 8.** PSD at the core (Interior) and near the exposed surface (Exterior) of samples after
696 120-days of carbonation (PC, BNC05 and BNC15)

697 **Fig. 9.** XRD patterns at the core (Int) and near the outer rim (Ext) of PC and BNC15
698 samples exposed to scCO2 for 120 days.

699 **Fig. 10.** Development of the compressive strength (red) and Young's modulus (blue) of PC
700 (a), BNC05 (b) and BNC15 (c) over the carbonation time.

701 **Fig. 11.** PSD variation in time for a point near the exposed surface of PC samples. Non-
702 carbonated (Time 1), 15 days of carbonation (Time 2), 30 days of carbonation (Time 3) and
703 120 days of carbonation (Time 4).

704 Table 1. MIP Tests

Test	Reference	BNC [%]	Carbonation days
1	PCNC	0	0
2	PC30Ext	0	30
3	PC120Int	0	120
4	PC120Ext	0	120
5	BNC05NC	0.05	0
6	BNC0530Ext	0.05	30
7	BNC05120Int	0.05	120
8	BNC05120Ext	0.05	120
9	BNC15NC	0.15	0
10	BNC1530Ext	0.15	30
11	BNC15120Int	0.15	120
12	BNC15120Ext	0.15	120

705 Table 2. Average values of density and mass absorption after carbonation

		30 Days of carbonation		120 Days of carbonation	
Samples (I and II)	Initial density [g/cm^3]	Mass Uptake [g]	Density variation [%]	Mass Uptake [g]	Density variation [%]
PC	1.99	2.7	+1.4	4	+2.5
BNC05	1.93	2.8	+1.5	3.3	+2
BNC15	1.97	2.1	+1.3	7.5	+3.6

706 Table 3. Relative percentage of the crystalline phases before and after exposure

Crystalline phase (%)	PC			BNC15		
	NC	120Int	120Ext	NC	120Int	120Ext
Portlandite	50	52	5	63	55	1
Katoite	16	23	-	14	26	-
Gypsum	-	Traces	Traces	-	-	-
Brownmillerite	16	11	9	12	10	5
Tobermorite	-	-	-	Traces	Traces	-
Brucite	-	3	-	-	Traces	-
Okenite	5	-	-	-	-	-
Calcite	13	10	12	10	8	9
Aragonite	-	Traces	73	-	-	85

707

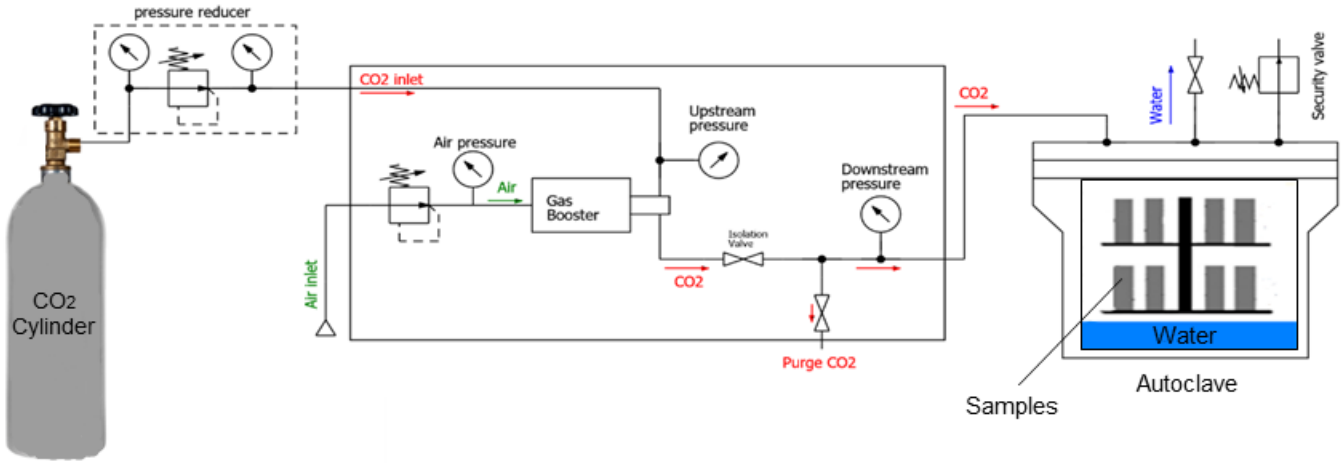

708

709 **Fig. 1.** Carbonation system

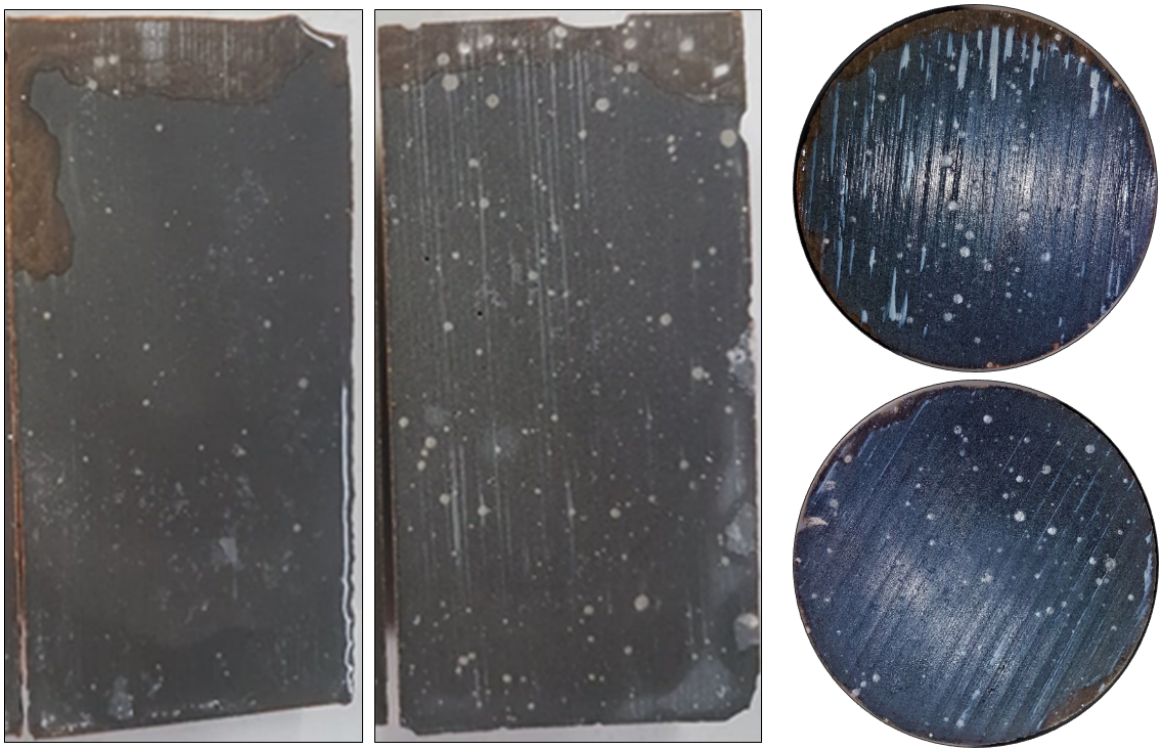

710

711 **Fig. 2.** PC (Left longitudinal and top radial samples) and BNC05 (right longitudinal and
712 inferior radial) samples after 120 days of carbonation
713

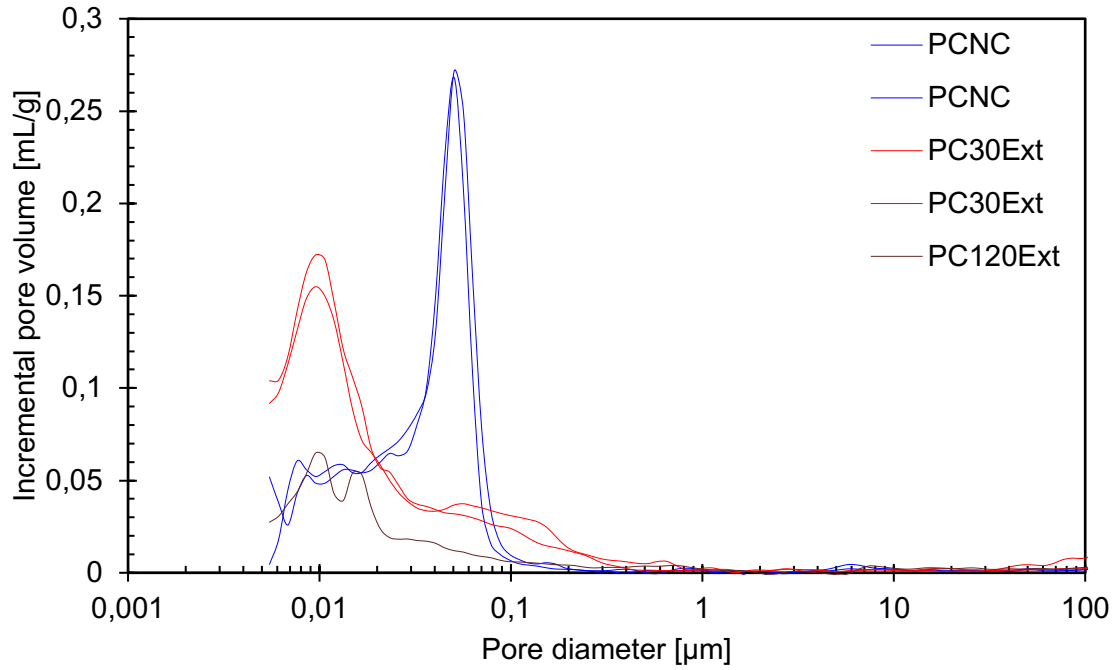

714

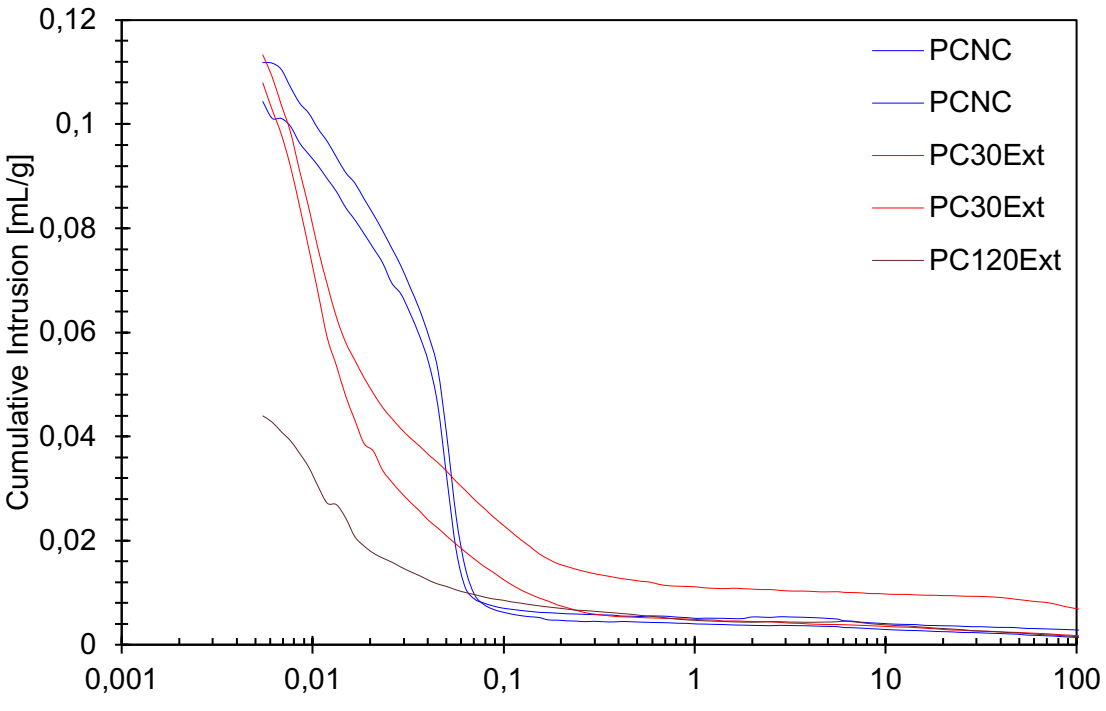

715
716 **Fig. 3.** Cumulative intrusion volume and PSD of PC.
717

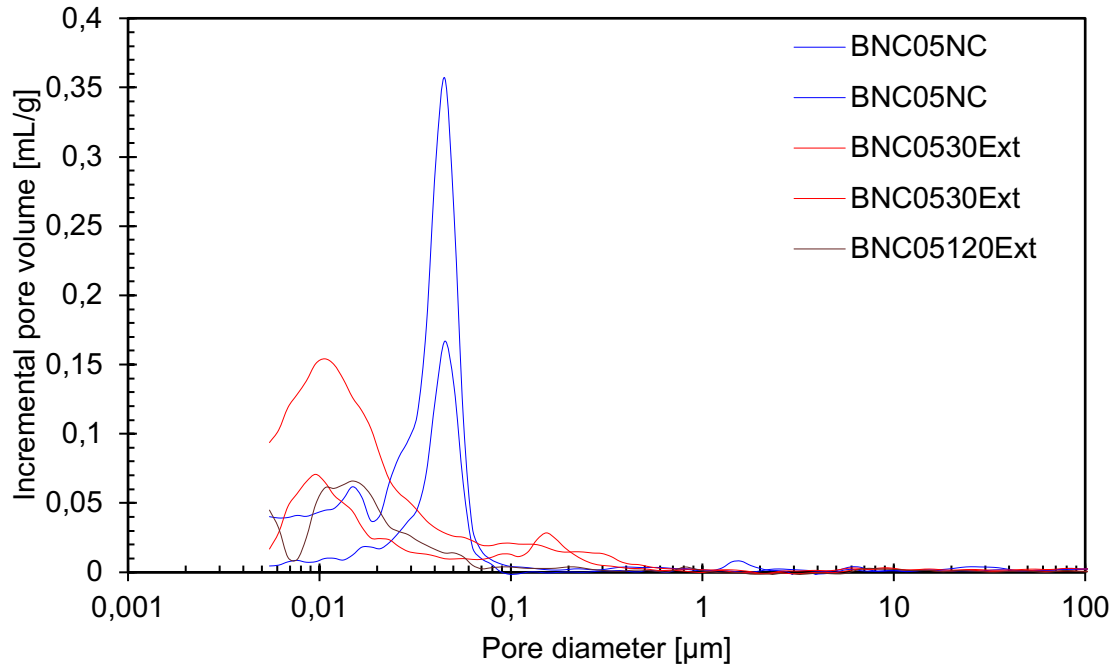

718

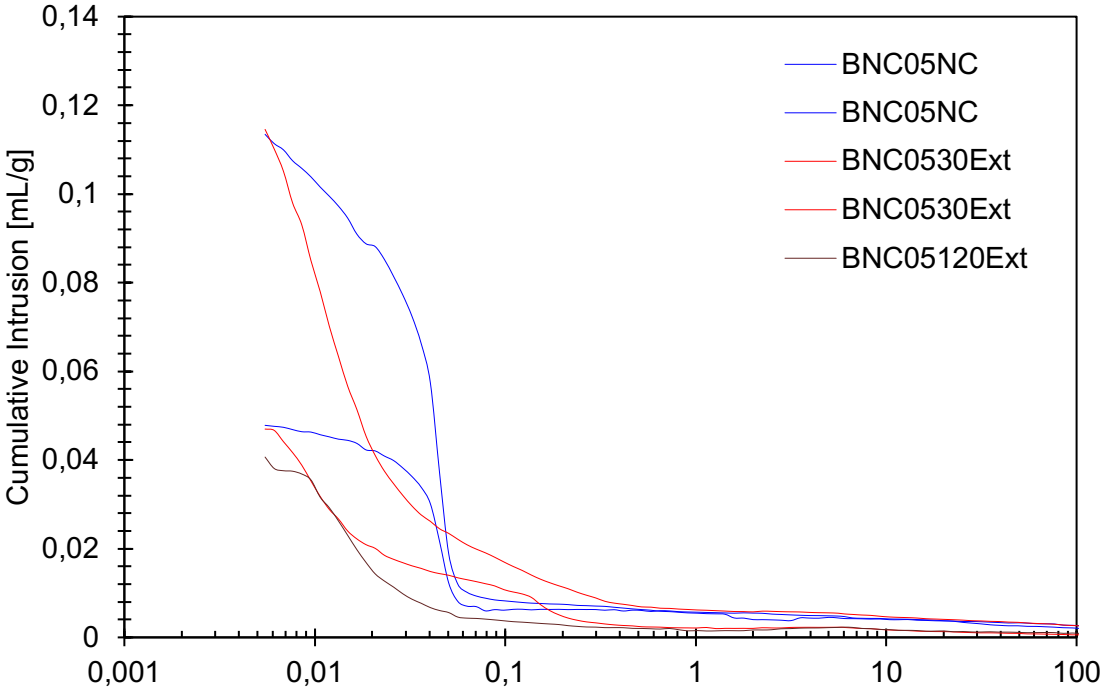

719

720 **Fig. 4.** Cumulative intrusion volume and PSD of BNC05

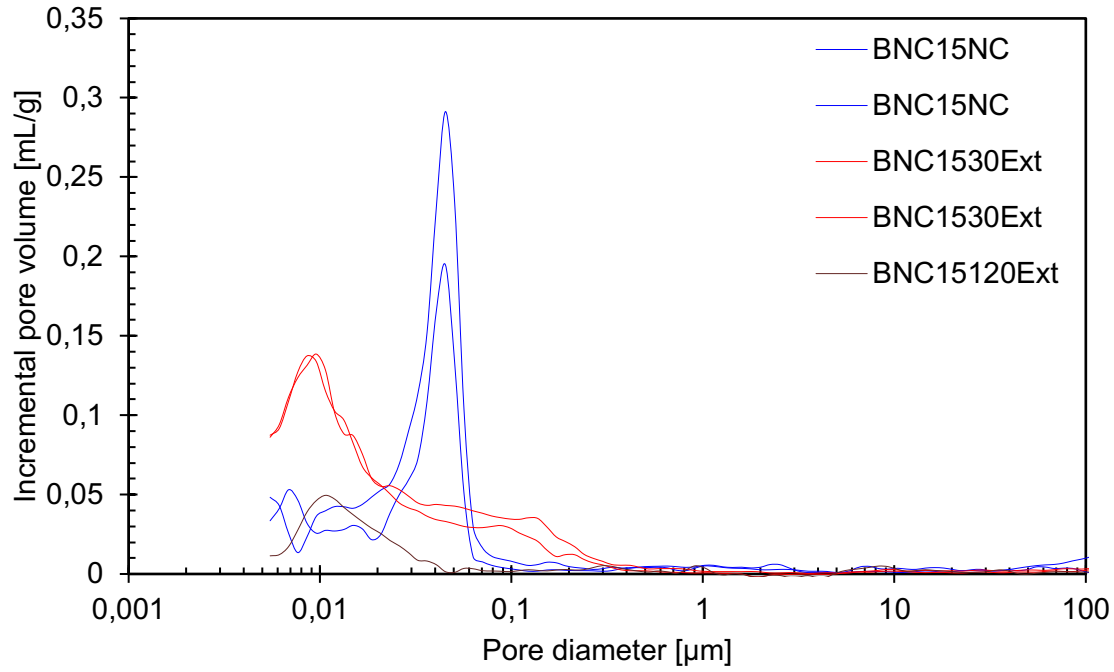

721

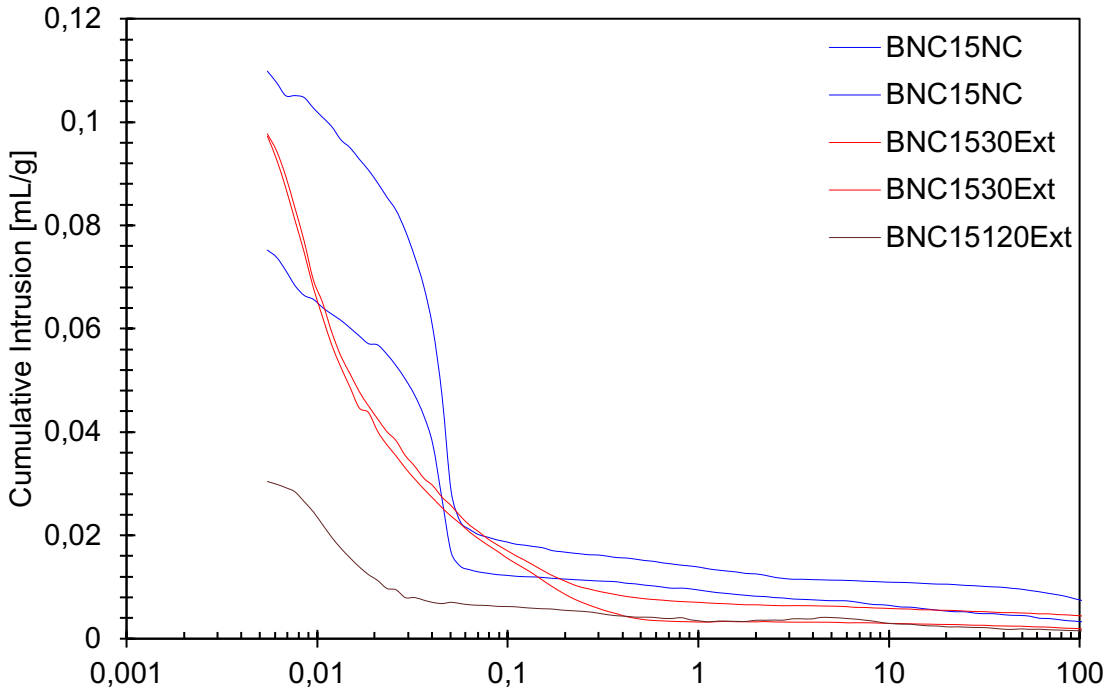

722

723 **Fig. 5.** Cumulative intrusion volume and PSD of BNC15

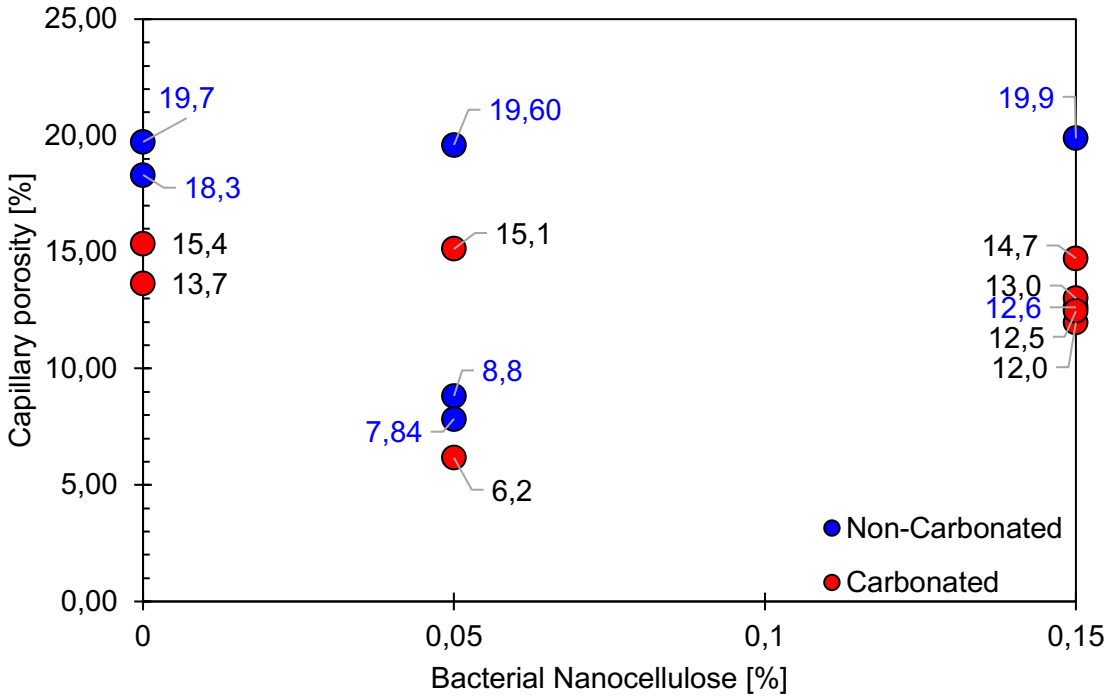

Fig. 6. Capillary porosity of non-carbonated samples and 30-days carbonated samples (PC, BNC05 and BNC15)

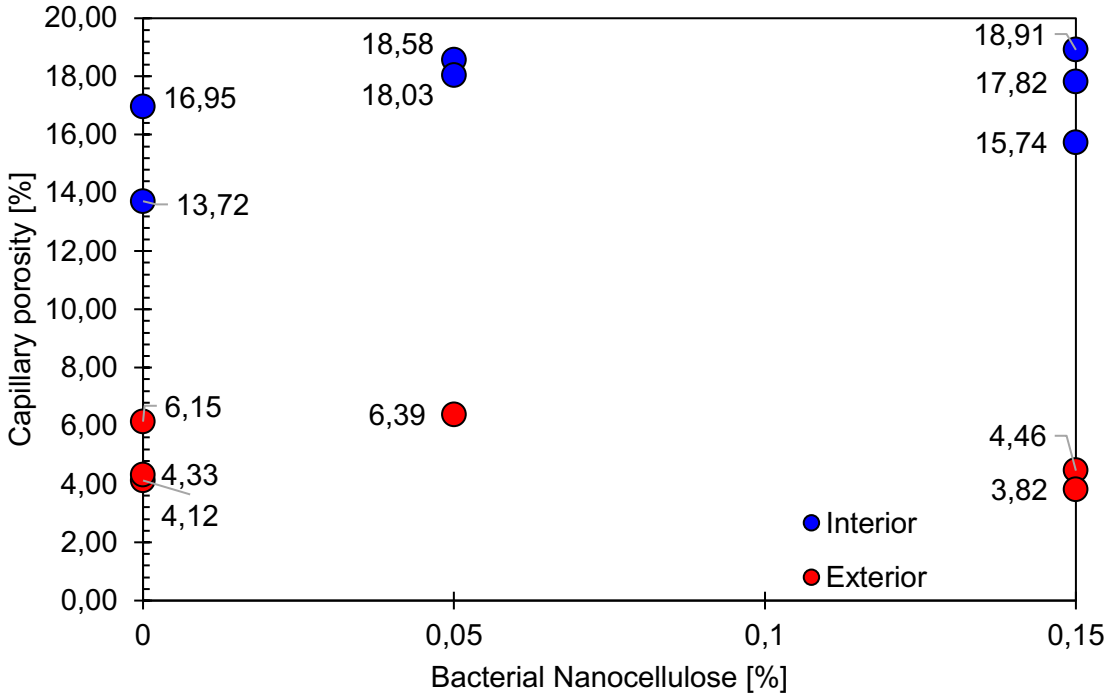

730 **Fig. 7.** Capillary porosities at the core (Interior) and near the exposed surface (Exterior) of

731 samples after 120-days of carbonation (PC, BNC05 and BNC15).

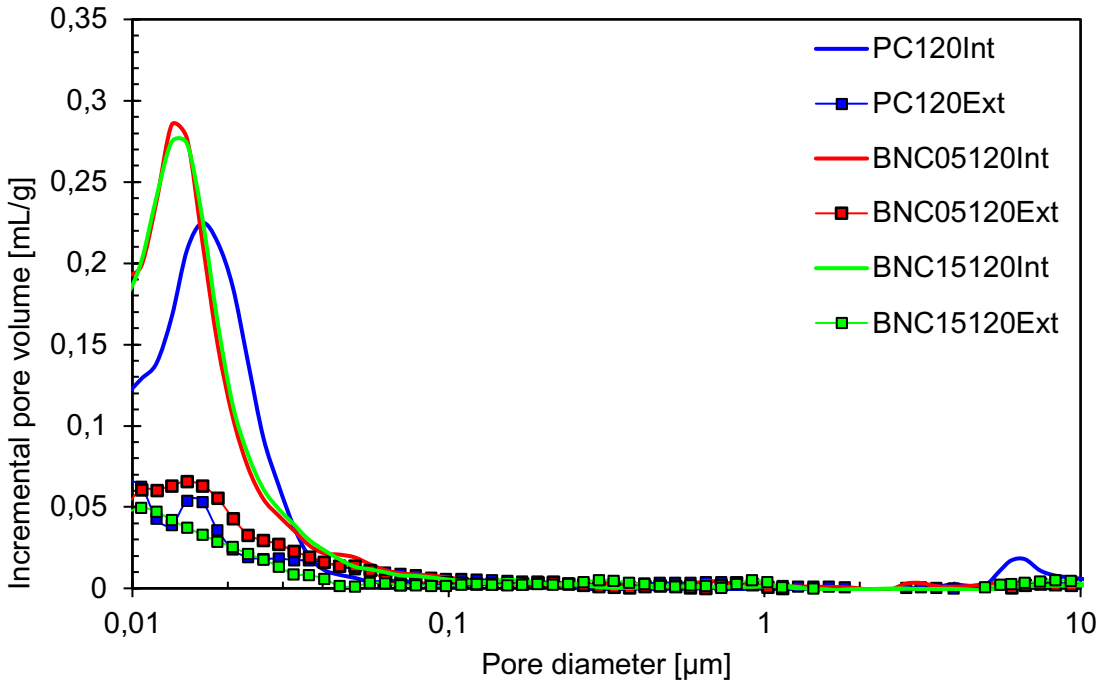

732

733 **Fig. 8.** PSD at the core (Interior) and near the exposed surface (Exterior) of samples after

734 120-days of carbonation (PC, BNC05 and BNC15)

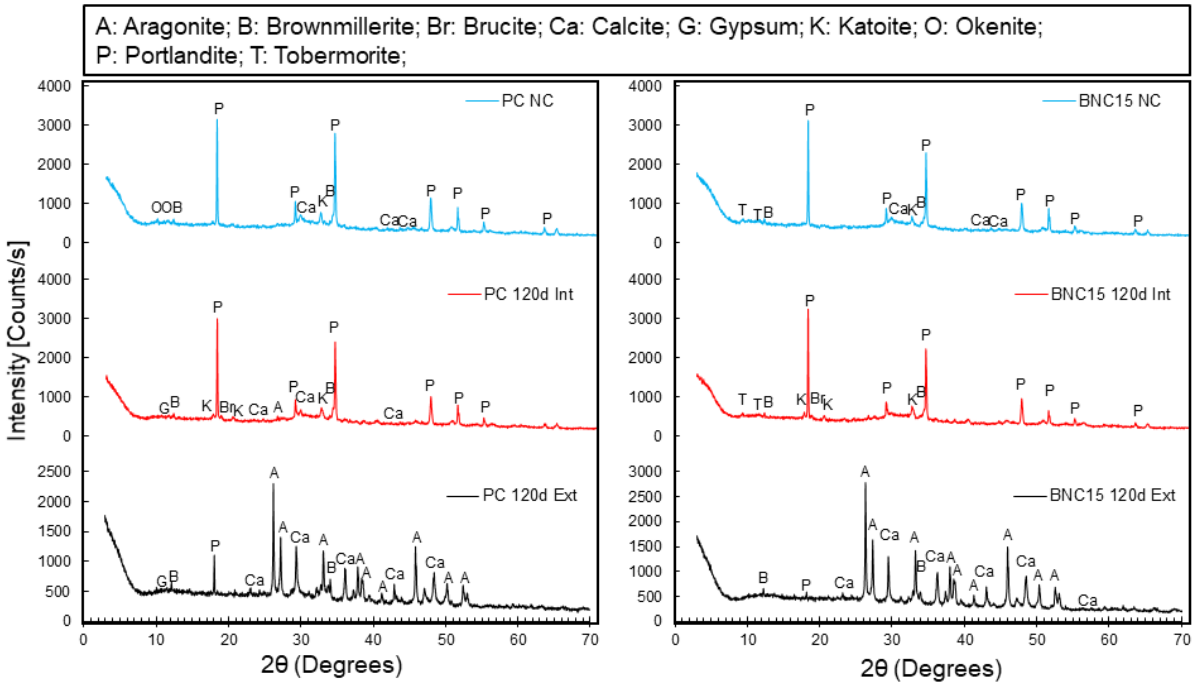

735

736 **Fig. 9.** XRD patterns at the core (Int) and near the outer rim (Ext) of PC and BNC15

737 samples exposed to $scCO_2$ for 120 days.

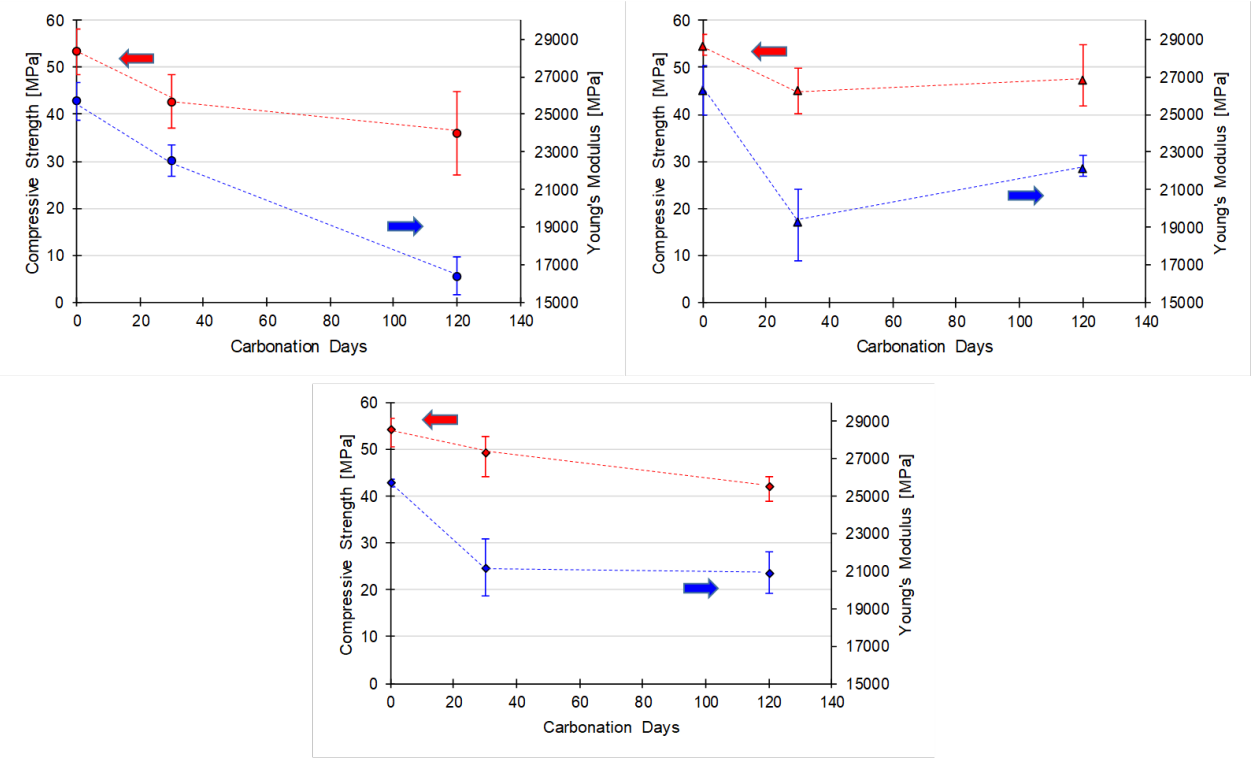

738

739 **Fig. 10.** Development of the compressive strength (red) and Young's modulus (blue) of PC

740 (a), BNC05 (b) and BNC15 (c) over the carbonation time.

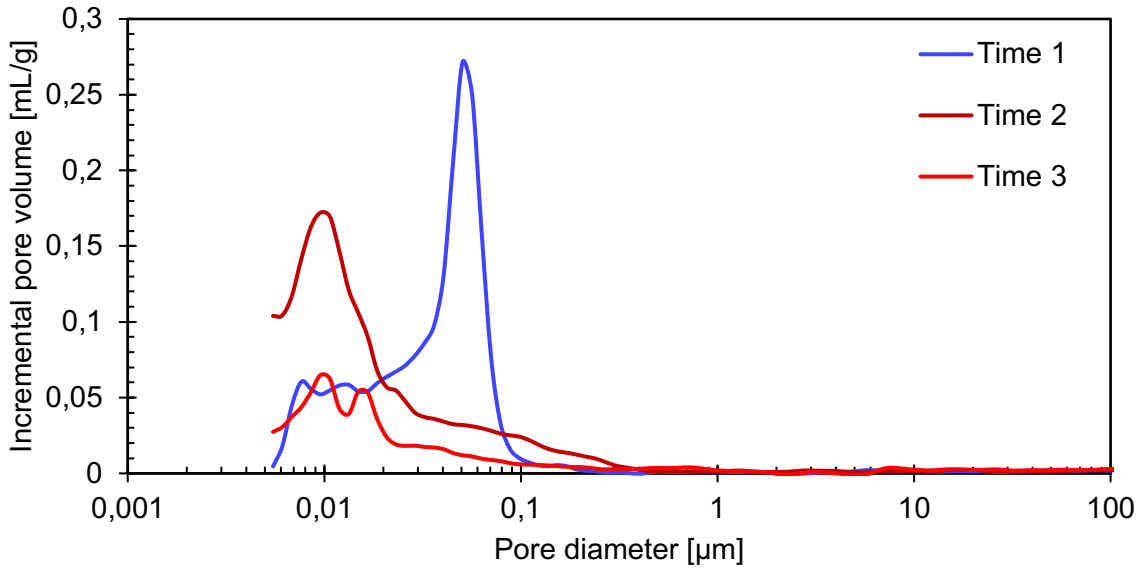

741

742 **Fig. 11.** PSD variation in time for a point near the exposed surface of PC samples. Non-

743 carbonated (Time 1), 30 days of carbonation (Time 2) and 120 days of carbonation (Time

744 3).

745